Nanomechanical characterization of recalcitrant foulants and hollow fibemembranes in ultrafiltration systems

Article *in* Desalination and Water Treatment · October 2018

DOI: 10.5004/dwt.2018.23257

CITATIONS
2

READS
602

5 authors, including:

Alexander Franz Keucken
Lund University
25 PUBLICATIONS **600** CITATIONS
SEE PROFILE

Leonardo Gutierrez
Universidad del Pacífico (Ecuador)
63 PUBLICATIONS **1,750** CITATIONS
SEE PROFILE

Cyril Aubry
Khalifa University
41 PUBLICATIONS **912** CITATIONS
SEE PROFILE

Teresa Vera
Corporación Universidad de la Costa
17 PUBLICATIONS **35** CITATIONS
SEE PROFILE

Desalination and Water Treatment
www.deswater.com

doi: 10.5004/dwt.2018.23257

136 (2018) 49–64
December

Nanomechanical characterization of recalcitrant foulants and hollow fiber membranes in ultrafiltration systems

Leonardo Gutierrez[a,b,*], Alexander Keucken[c,d], Cyril Aubry[e], Teresa Vera San Martin[b], Jean-Philippe Croue[a]

[a]*Curtin Water Quality Research Centre, Department of Chemistry, Curtin University, Australia, Tel. +32 468 358 104; email: leonardo.gutierrezgarces@curtin.edu.au (L. Gutierrez), Tel. +61 438 860 666; email: jean-philippe.croue@curtin.edu.au (J.-P. Croue)*
[b]*Facultad del Mar y Medio Ambiente, Universidad del Pacifco, Guayaquil, Ecuador, Tel. +593 99 617 9664; email: teresa.vera@upacifico.edu.ec (T.V. San Martin)*
[c]*Vatten & Miljö i Väst AB (VIVAB), Falkenberg, Sweden, Tel. +46 (0)70 598 99 62; email: Alexander.Keucken@vivab.se*
[d]*Water Resources Engineering, Faculty of Engineering, Lund Technical University, Lund, Sweden*
[e]*Masdar Institute of Science and Technology, Masdar City, Abu Dhabi, United Arab Emirates, Tel. +971 2 810 9534; email: caubry@masdar.ac.ae*

Received 15 July 2018; Accepted 9 October 2018

ABSTRACT

Long-term nanomechanical changes of polymeric ultrafiltration (UF) membranes caused by fouling/cleaning agents in water treatment are not well established in the literature. The goal of this study was to investigate the nanomechanical properties of polymeric UF hollow fiber membranes operating at a pilot-scale for 449 d and subjected to a low-quality feed (i.e., high turbidity/TOC content). Quantitative nanomechanical mapping technique was used to measure the deformation, dissipation, modulus, adhesion, and roughness of the polymeric structures of commercial Aquaflex virgin membranes, harvested membranes, and foulant layers. Results indicated that the recalcitrant and heterogeneous nature of the foulants absorbed on harvested membranes showed low elastic properties, and high modulus, adhesion, and roughness. The strong affinity of these foulants towards membrane surface would alter membrane characteristics and influence subsequent fouling behaviour. The cleaning process and extended operation did not significantly affect the nanomechanical properties of membranes. Despite the low-quality feed, the three modules were only subjected to 37 chemical-enhanced backwashes and filtered a total volume of 2.155 m^3. These results indicate the importance of operating conditions (i.e., frequency of backwash/cleaning/disinfection steps) and feed quality on the long-term changes of UF membranes and would assist in identifying research directions that are necessary to minimize membrane fouling/ageing.

Keywords: Quantitative nanomechanical mapping; Ultrafiltration; Hollow fiber membranes; Fouling; Chemical cleaning

1. Introduction

Conventional treatment of surface water involves a combination of chemical and physical processes, for example, sand filtration, flocculation, coagulation, and disinfection. Nevertheless, bacterial content, turbidity, and organic matter concentration of surface water are subjected to seasonal fluctuations [1]; resulting in high operational costs. Despite its limited chemical and heat resistances, polymeric membrane ultrafiltration (UF) is a widely used tool for surface water treatment due to its low footprint and chemical requirements, low-pressure filtration, and

* Corresponding author.

flexibility against water quality fluctuation. UF acts as a physical barrier that delivers a disinfected and clear product [2], and it is increasingly replacing conventional water treatments. However, membrane fouling remains as a persistent issue that decreases the efficiency of the process.

Fouling is caused by the adsorption of particulate/dissolved materials, leading to an increase in hydraulic filtration resistance and frequent maintenance [3]. Natural organic matter (NOM) is a key and ubiquitous component of fouling in UF [4]. NOM is the complex and heterogeneous microbial product of the decay of plants and vegetables [5]. NOM characteristics are highly dependent on its origins; however, humic substances are predominant in surface waters [5,6]. UF fouling occurs as: membrane surface fouling and internal pore fouling [7]. While the former is caused by the adsorption of NOM and colloids (i.e., often reversible and controlled by hydrodynamic flushing), the latter is produced by NOM adsorption (i.e., physically/chemically difficult to desorb). Despite extensive research, the specific contribution of these two mechanisms to membrane fouling and flux decrease is not yet clear. Preventive measures to interfere with NOM fouling (e.g., coagulation, oxidation, ion exchange, carbon adsorption) are aimed to decrease their interactions with membranes, change the size distributions of contaminants, and to suppress microbial activity [4]. Analytical techniques used for studying fouling in UF systems include scanning electron microscopy, atomic force microscopy, Fourier-transform infrared spectroscopy, nuclear magnetic resonance, and surface-enhanced Raman spectroscopy [8]. Briefly, polysaccharide-like compounds have shown high affinity for membrane surfaces; where metals (e.g., Fe, Mn) have been reported to induce irreversible fouling [9]. Divalent cations (Ca^{2+}) and high ionic strength were observed to enhance HS fouling by cation bridging, lowering electrostatic interactions, and by inducing conformational changes in the organic molecules [10]. Due to the complexity and heterogeneity of the feeds, it is difficult to isolate individual/dominant mechanisms [11]. Synergistic mechanisms between organics of different characteristics may occur, leading to a more recalcitrant fouling [12]. Reversible fouling has been reported to lose its reversibility after a long period of operation; while irreversible fouling fraction gradually increased [13]. As a result, the desorption of these molecules turns thermodynamically unfavourable [14], and fouled membranes cannot be restored without chemical cleaning.

UF polymeric membranes are mechanically and chemically stressed due to the frequency and the harshness of cleaning conditions, resulting in membrane degradations [15]. Although there are physical cleaning methods that provide more sustainable conditions for decreasing fouling (e.g., air scrubbing, hydraulic/surface backwashing), cleaning agents can cause irreversible damages in membrane properties and performances over the long term [16,17]. NaOCl is one of the most detrimental chemical for polymeric membranes [18], as shown in both static and accelerated ageing conditions [19,20]. Despite their chemical stability (pH, temperature range, and resistance to oxidation), the mechanical properties of PSf and PES membranes have been impacted by NaOCl [21]. At a microscopic scale, the polymer modification by acid/alkaline cleaning has been identified by FTIR-ATR (aromatic compounds), EDX, streaming potential, and F-Raman (deprotonation of $–CH_2$ and the formation of C=C double bonds) [17,22–24]. On the other hand, quantitative changes in UF membrane macroscopic properties have been monitored by mechanical strength (e.g., ultimate/loss of elongation at break, signs of embrittlement, yield/tensile strength, elasticity) and permeability tests [25,26]. These previous studies have shown the importance of coupling macroscopic and microscopic characterization methods. However, long-term changes of UF polymeric membranes caused by fouling/cleaning agents in industrial processes are not well established in the literature [27], and require more research. For instance, the high concentration of cleaning reagents applied to UF membranes for a short time during accelerated ageing experiments are not representative of industrial conditions (i.e., lower concentrations for a significant cumulated contact time, and the presence of foulants adsorbed on membrane surface).

Therefore, the goal of this study was to investigate the long-term changes of the nanomechanical properties of UF hollow fiber membranes operating at a pilot-scale for 449 d, and subjected to a low-quality feed (i.e., treatment of the backwash water of a primary UF stage unit showing high turbidity and high TOC content). PeakForce™ quantitative nanomechanical mapping (QNM) technique was used to measure the deformation, dissipation, modulus, adhesion, and roughness of the polymeric structures of commercial Pentair X-Flow Aquaflex virgin membranes, harvested membranes, and foulant layers. Additionally, this QNM analysis assisted in the nanomechanical description of UF irreversible fouling. A rigorous statistical analysis was conducted to assess the change in membrane characteristics. Surface imaging by SEM coupled with energy-dispersive X-ray spectroscopy (EDS) was used as complementary tools to study membrane surfaces. The permeability (i.e., macroscopic property) of harvested membranes was measured and compared with QNM results. The use of macro/microscopic, spectroscopic, and nanomechanical methods in the current study will assist in acquiring information to understand UF membrane fouling and ageing in long-term industrial operations, and to generate a global vision of membrane ageing.

2. Materials and methods

2.1. Pilot-scale plant description and operation

The pilot system operated from January 2015 to August 2016 and involved a coagulation system followed by a two-stage membrane UF process (Kvarnagården Water Treatment Plant, Varberg municipality, Sweden). The raw water feeding this coagulation–UF pilot system consisted of 80% surface water (i.e., oligotrophic lake) and 20% groundwater. The treatment capacity of the pilot system was 170 m^3/d. While the coagulation stage created flocs, the primary UF membrane stage (i.e., horizontal dead-end filtration with two Pentair X-Flow XIGA hollow fiber membrane modules) provided NOM retention and barrier function. The backwash water of this primary UF stage was treated by a second stage UF membrane system (i.e., vertical dead-end filtration, inside-out mode, with one Pentair X-Flow AQUAFLEX hollow fiber membrane module: Sulfonated polyethersulfone PES, 100 kDa MWCO, temperature range

0°C–40°C, pH range 1–13 during cleaning), which increased the recovery of the plant to >99%. Caustic/acidic cleaning conditions (i.e., chemical enhanced backwash [CEB], H_2SO_4, NaOH, and NaOCl), module replacements, operational conditions during long-term test runs, and membrane key performance parameters of the secondary UF stage were summarized in Tables S1 and S2.

2.2. Feed water characteristics of the secondary UF module and membrane samples

The membrane samples were harvested from the secondary UF unit operating in vertical dead-end top-bottom filtration inside-out mode (i.e., one Pentair X-Flow Aquaflex hollow fiber membrane module). The backwash water of the primary UF unit was the feed water of the secondary UF unit; thus, displaying a very low quality, that is, turbidity: 20.0–25.0 NTU; DOC: 4.0–4.9 mg C/L; TOC: 22.0–28.0 mg C/L (Table S3). The total filtration volume was 2,155 m^3 (Table S2). The UF module was harvested after a final CEB. Membrane samples were collected at specific locations of the secondary UF module (Fig. S1), and termed as: (a) Aquaflex top, (b) Aquaflex middle, and (c) Aquaflex bottom. Virgin membrane samples were also investigated and termed as (d) Aquaflex virgin.

2.3. Membrane sample preparation, SEM/EDS analysis, and permeability tests

Using an optic microscope and under aseptic conditions, harvested (Aquaflex top, Aquaflex middle, and Aquaflex bottom) and virgin (Aquaflex virgin) UF hollow fiber membrane samples were dissected in halves for scanning electron microscopy (SEM), EDS, and Atomic Force Microscopy (AFM) analysis. Additionally, virgin membranes were soaked in ultrapure water overnight to remove preservatives.

A NovaNano SEM in immersion mode (FEI, Netherlands) was used to capture high-resolution images of membranes. Briefly, to avoid any charging effect due to the non-conductive nature of the membranes, samples were coated by sputtering a 10-nm thick layer of Au/Pd (PECS 628, Gatan). Cross-sectioning of membrane samples were performed by focused ion beam (FIB) technique (Quanta 3D dual beam FIB, FEI, Netherlands). Similarly, a 50-nm Au/Pd protective layer was deposited on the membrane surface to preserve it from any damage caused by the ion beam. An additional 2.5 μm thick protective layer was deposited using the gas injection system; then, samples were etched with the FIB. The generated cross-section was coated with a 10-nm thick layer of Au/Pd for further high-resolution SEM imaging. The pore size distribution of virgin membrane surface was calculated by ImageJ software (National Institute of Health, United States) using a threshold filter to discriminate pores from the membrane. The mean (μ) pore size distribution was statistically determined by probability density functions. A SEM/EDS Quanta 250 (FEI, Netherlands; EDS detector, EDAX) working in environmental mode (ESEM) was used to perform chemical analyzes of membrane surfaces (i.e., virgin and harvested membranes). The pressure of water vapor was maintained at a constant value of 500 Pa allowing to remove charging effects due to the non-conductive nature of the membranes. The hydraulic permeability of single hollow fibers was measured (i.e., flow experiments). The permeability of harvested membranes was compared with that of virgin membranes. These macroscale properties of hollow fiber membranes were correlated to the microscopy results.

2.4. Morphological analysis by soft-tapping mode and QNM

An initial phase and topographic (morphological) analysis of (a) cross-section of membrane (i.e., resulting from the FIB process) (Fig. S2(a)), (b) external outermost layer (Fig. S2(b)), and (c) membrane (inner) surface (Fig. S2(a)) (i.e., hollow fiber membranes operated in inside-out mode) by Soft Tapping Mode™ (Bruker, United States) in air conditions was conducted. TESPA AFM probes (silicon tip, k: 42 N/m, f: 320 kHz, Bruker, United States) were selected. While this topographic analysis provided information of the morphology of samples, phase analysis allowed a chemical mapping of membrane surfaces based on material differences.

A Dimension FastScan AFM (Icon Head, Bruker, United States) was used for QNM analysis in electrolyte solution of the following membrane samples: (a) Aquaflex top, (b) Aquaflex middle, (c) Aquaflex bottom, and (d) Aquaflex virgin. A 1-mM NaCl electrolyte solution was prepared with ultrapure water and analytical grade reagents, and then filtered through a 0.22 μm membrane. Due to the soft polymeric nature of the membrane samples, Sharp Nitride Lever AFM probes (SNL-10 A, k: 0.35 N/m, silicon nitride cantilever, Bruker, United States) were selected to induce enough deformation without damaging the sample while still retaining their sensitivity. Prior to QNM experiments, the deflection sensitivity of the AFM probes was measured in air conditions and using a freshly cleaved mica surface as a control substrate, the spring constant of the cantilevers was determined by the thermal tuning method [28], and the radius of curvature of the AFM probes was calculated by scanning a titanium model surface in air conditions via tip qualification function in the NanoScope Analysis Software V1.5 (Bruker, United States).

The previously dissected membrane samples (Aquaflex top, Aquaflex middle, Aquaflex bottom, and Aquaflex virgin) were immobilized concave up on a glass slide using double-sided tape, where the inner surface was examined with the AFM high-resolution camera to locate suitable scanning areas (Fig. S2(a)). To generate high-resolution images, QNM images of the membrane samples were acquired at a 0.5 kHz scan rate, over an area from 2 × 2 μm to 5×5 μm, and at 512 samples/line. Also, the Peak Force Setpoint was automatically controlled by the software (ScanAsyst Auto Control was set ON). From 30 to 35 locations were randomly selected in every hollow fiber membrane sample; where the following parameters (channels) were simultaneously recorded: topography, peak force error, adhesion, deformation, dissipation, and LogDMT modulus. Briefly, while the deformation channel measures the maximum deformation (nm) of the polymeric structures of the membrane caused by the AFM probe during approaching regime, the LogDMT modulus channel (i.e., following the Derjaguin-Muller-Toporov-DMT modified Hertzian model) describes the tensile elasticity of the polymeric structures as the logarithm of the elastic modulus [29]. The adhesion channel measures the maximum adhesion

force (nN) between the AFM probe and membrane surface during the retraction regime. The peak force error channel generates a map of the peak force measured during the scan. The mechanical energy lost per approaching-retracting cycle is described by the dissipation channel. Specifically, low dissipation values correspond to elastic deformation, while high dissipation values to plastic deformation. Image quadratic mean (R_q) analysis was used to process every peak force, height, LogDMT modulus, adhesion, dissipation, and deformation data (NanoScope Software V1.5, Bruker, United States). The R_q values were statistically analyzed by probability density functions, where mean (μ) and variance (σ) were extracted. This analysis was conducted for both membrane surfaces and fouling layers.

3. Results and discussion

3.1. Surface morphology of virgin membrane samples

The morphological analysis of Aquaflex virgin included (a) cross-section of membrane, (b) external outermost layer (supporting layer), and (c) membrane (inner) surface; all displaying different characteristics. Briefly, height sensor (Fig. 1(a)) AFM images of the cross-section of Aquaflex virgin showed a rough and heterogeneous topography. The roughness (R_{RMS}) of Aquaflex cross sections was calculated as 71.9 ± 25.7 nm (n = 6). SEM images of Aquaflex virgin cross-section evidenced a similar morphology to those of AFM (Fig. 1(b)). On the other hand, height sensor and SEM images of the external outermost layer (i.e., supporting layer) displayed a rough surface (R_{RMS} > 100 nm) containing pores of φ between approximately 1 μm and 1.25 μm (Figs. 1(c) and (d)).

The morphology of Aquaflex virgin membrane surface as viewed in SEM images (Fig. S3(a)) was similar to those of the cross-section (Fig. 1(b)), although the polymeric structures

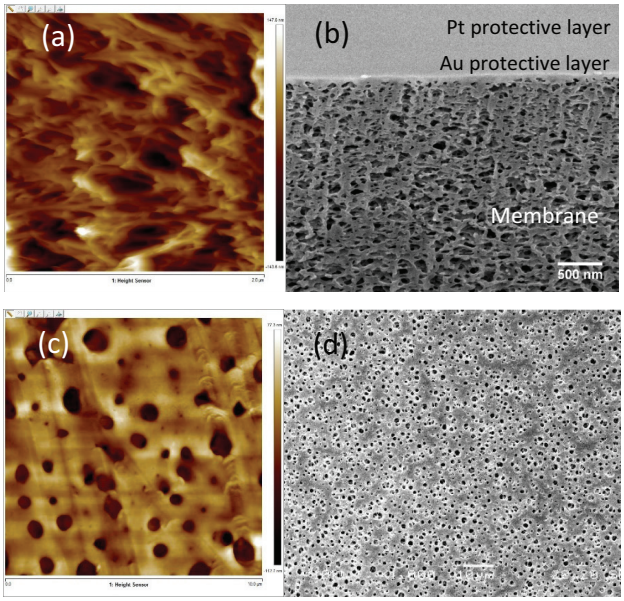

Fig. 1. (a) Height sensor AFM image and (b) SEM image of the cross-section of Aquaflex virgin. (c) High sensor and (d) SEM micrograph of external outermost layer of Aquaflex virgin.

of the membrane surface showed more compact (i.e., as also evidenced by a lower R_{RMS} roughness compared with that of the cross section). A statistical analysis by probability density function was used to calculate pore size distribution of Aquaflex virgin surface from the SEM images (Fig. S3(a)) using ImageJ software (Fig. S3(b)). The mean pore size was determined as 6.4 nm (i.e., σ: 0.63 and R^2: 0.99) (Fig. S3(c)) and was smaller than those reported by the manufacturer (i.e., 20 nm nominal pore size) and previous studies [7]. The roughness (R_{RMS}) of Aquaflex virgin was measured as 19.3 ± 3.2 nm (n = 6) by topography images (3D-height sensor) in soft-tapping mode in air. Remarkably, topography and phase images revealed the physically and chemically heterogeneous nature of the surface of Aquaflex virgin, respectively (Figs. S4(a) and (b)).

3.2. Nanomechanical properties of fouling layers and hollow fiber membranes

3.2.1. Aquaflex virgin hollow fiber membranes

As a first step, the surface of Aquaflex virgin was investigated by QNM (Fig. 2). All the properties of Aquaflex virgin were statistically processes by normal probability distributions (Fig. S5). The mean (μ) roughness, adhesion, peak force error, dissipation, LogDMT modulus, and deformation of Aquaflex virgin were 16.7 nm, 0.36 nN, 0.18 nN, 59.7 eV±, 0.067 Log[Pa]±, and 7.7 nm (Table 1, Fig. S5), respectively. The roughness and the morphology (Fig. 2(a)) of Aquaflex virgin, as recorded by QNM-height sensor, was similar to that of soft-tapping mode and high-resolution SEM micrographs (Fig. S3(a)), respectively. Also, the low LogDMT modulus and dissipation values indicate a soft polymeric structure of elastic properties. The mechanical properties recorded for Aquaflex virgin were similar to those of previously studied XIGA UF-hollow fiber membranes [30]. Remarkably, QNM technique evidenced its capability in the discrimination of structural features differing from the surrounding polymeric structures, for example, areas of higher adhesion than those of the surrounding polymeric structures (Fig. 2(d)). The surface of polymeric membranes has been previously characterized by chemical force spectroscopy as physically and chemically heterogeneous [31]; thus, confirming the results of the current investigation. The nanomechanical properties of Aquaflex virgin were further compared with those of harvested membranes (i.e., showing clean surfaces) and foulant layers.

3.2.2. Quantitative nanomechanical mapping of foulant layers

The secondary UF module operated for 449 d, was subjected to 37 CEBs, filtered a total volume of 2.155 m^3, and was harvested after a final CEB (section 2.1 and Fig. S1). As a consequence, (a) foulant layers and (b) clean surfaces were both observed in harvested membranes. Interestingly, the presence itself of foulant layers after long-term operation and multiple harsh CEB processes (Tables S1 and S2) indicate the recalcitrant nature of the foulants observed and their possible irreversible adsorption [32]. This sub-section strictly focused on the nanomechanical properties and morphology of foulant layers.

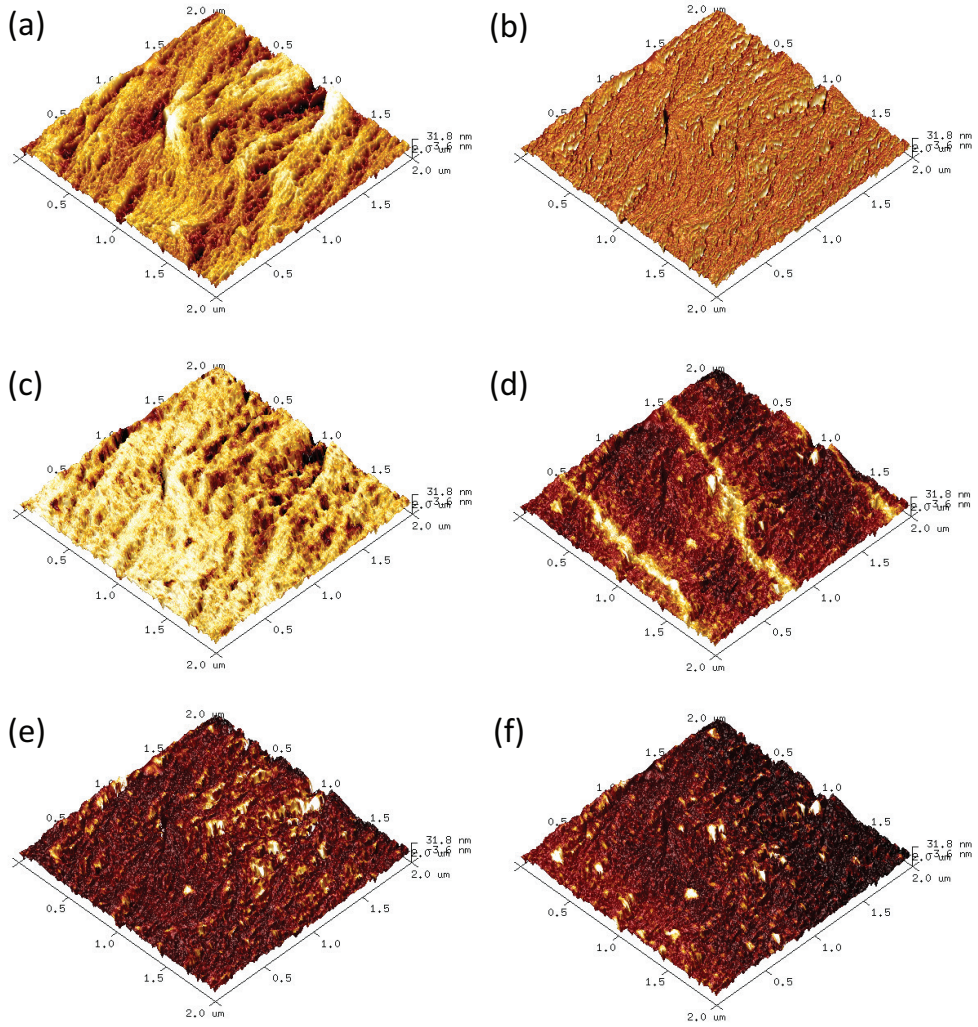

Fig. 2. (a) Height sensor, (b) peak force error, (c) LogDMT modulus, (d) adhesion, (e) deformation, and (f) dissipation images of Aquaflex virgin membrane. Scan area: 2 × 2 μm.

The foulant layers observed on harvested membranes (i.e., Aquaflex top, Aquaflex middle, and Aquaflex bottom) showed heterogeneous morphologies (Fig. 3(a)), surface characteristics, and mechanical properties (Fig. 4). Fouling layers were recorded totally covering scanning areas, where micro-cracks were also detected, that is, also evidenced in SEM images (Figs. S6(a) and (b)). Phase images of these fouling layers suggested materials of heterogeneous physicochemical characteristics (Fig. 3(b)). Interestingly, these micro-cracks (i.e., observed in Aquaflex top, middle, and bottom samples) provided crucial information regarding the thickness of the fouling layers. The depth of these crack ranged from 23 to 239 nm, where no membrane material was observed (Fig. 3(d)). This latter result suggests fouling layers thicker than 239 nm. SEM images of cross sections showed foulant layers of similar thickness (Fig. 3(c)). However, other samples showed cracks of few tens of nm where membrane material was detected (Figs. 3(e) and (f)), indicating the high heterogeneity of fouling layers in terms of thickness.

In addition to morphology, the mechanical properties of fouling layers highly differed from those of virgin membranes. As opposed to Aquaflex virgin, the nanomechanical properties of these foulant layers could not be statistically described by probability density functions because of the considerably high scatter in R_q values. Also, the maps of every property showed heterogeneous at the nanoscale (Fig. 4). Remarkably, QNM technique was capable of detecting specific regions of different adhesion, modulus, deformation, and dissipation properties within the fouling layer (Figs. 4(c)–(f)). These regions would potentially play a role in the subsequent fouling behaviour [32].

The mean roughness of the foulant layers was highly variable, for example, ranging from 51 to 130 nm (i.e., recorded at a 2 × 2 μm scan area); while the mean LogDMT modulus values ranged from 0.081 to 0.372 log[Pa]±. Although variable, the mean adhesion forces of these foulant layers were higher than those of Aquaflex virgin (e.g., ranging from 0.35 to 0.87 nN). The dissipation energies of these foulant layers ranged from 220 eV± to 598 eV±. As above-described, the fouling material of harvested Aquaflex membranes was highly variable in characteristics and nanomechanical properties. Nevertheless, these results clearly indicate that these fouling

Table 1
Values of mechanical properties of Aquaflex hollow fiber membrane samples. Mean (μ), variance (σ), and coefficient of determination (R^2) were obtained by probability density functions

	Roughness (nm)	Peak force (nN)	LogDMT modulus (log[Pa]±)	Adhesion force (nN)	Deformation (nm)	Dissipation (eV±)
Aquaflex virgin						
Mean (μ)	16.7	0.18	0.07	0.36	7.7	59.7
Variance (σ)	0.17	0.26	0.22	0.21	0.5	0.19
R^2	0.97	0.94	0.98	0.97	0.99	0.93
Aquaflex top						
Mean (μ)	6.2	0.18	0.06	0.37	4.0	48.7
Variance (σ)	0.32	0.36	0.14	0.14	0.48	0.5
R^2	0.98	0.97	0.99	0.99	0.99	0.97
Aquaflex middle						
Mean (μ)	11.1	0.14	0.07	0.46	4.5	52.6
Variance (σ)	0.4	0.07	0.43	0.24	0.3	0.31
R^2	0.98	0.93	0.95	0.82	0.98	0.98
Aquaflex bottom						
Mean (μ)	8.8	0.19	0.08	0.52	5.1	54.3
Variance (σ)	0.39	0.22	0.39	0.35	0.29	0.43
R^2	0.96	0.94	0.98	0.92	0.97	0.94

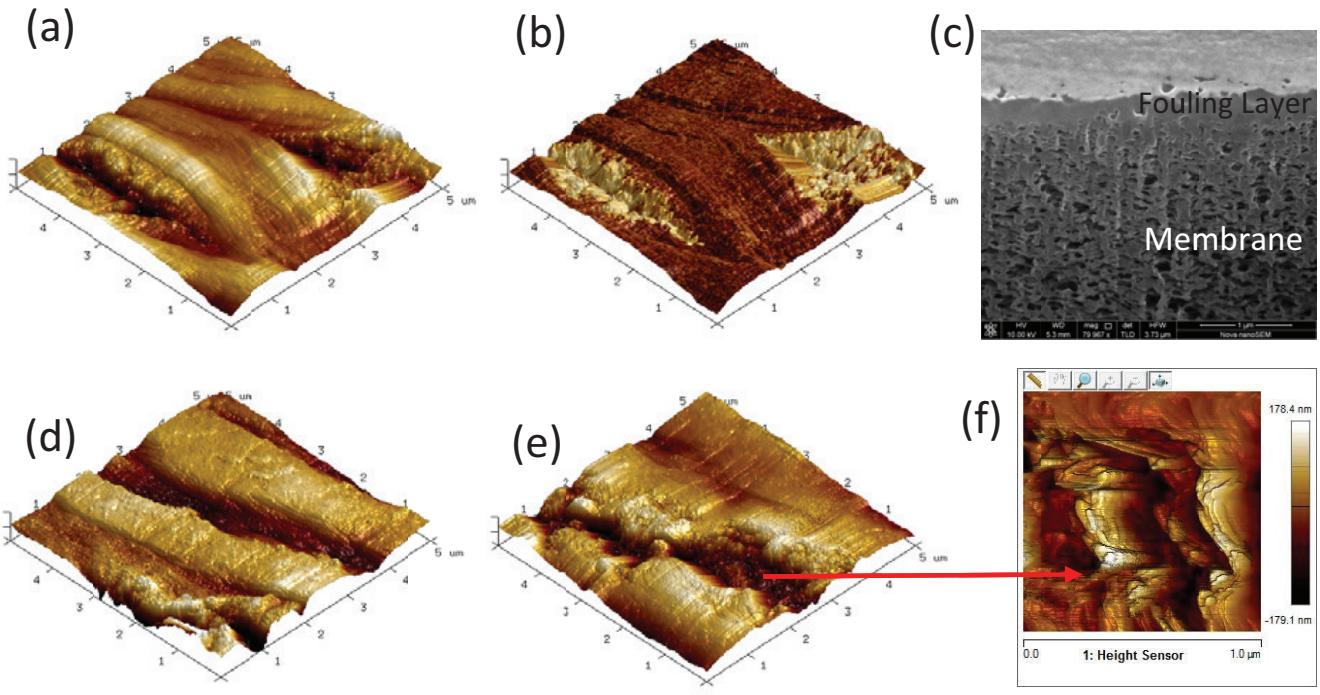

Fig. 3. (a) Height sensor and (b) phase images of fouled Aquaflex middle (scan area: 5 × 5 μm). (c) SEM image of cross section of Aquaflex middle showing a ~300 nm fouling layer. (d) Height sensor of fouled Aquaflex membrane (scan area: 5 × 5 μm). Height sensor of (e) fouled Aquaflex membrane showing micro-cracks (scan area: 5 × 5 μm) and exposing (f) membrane surface (scan area: 1 × 1 μm).

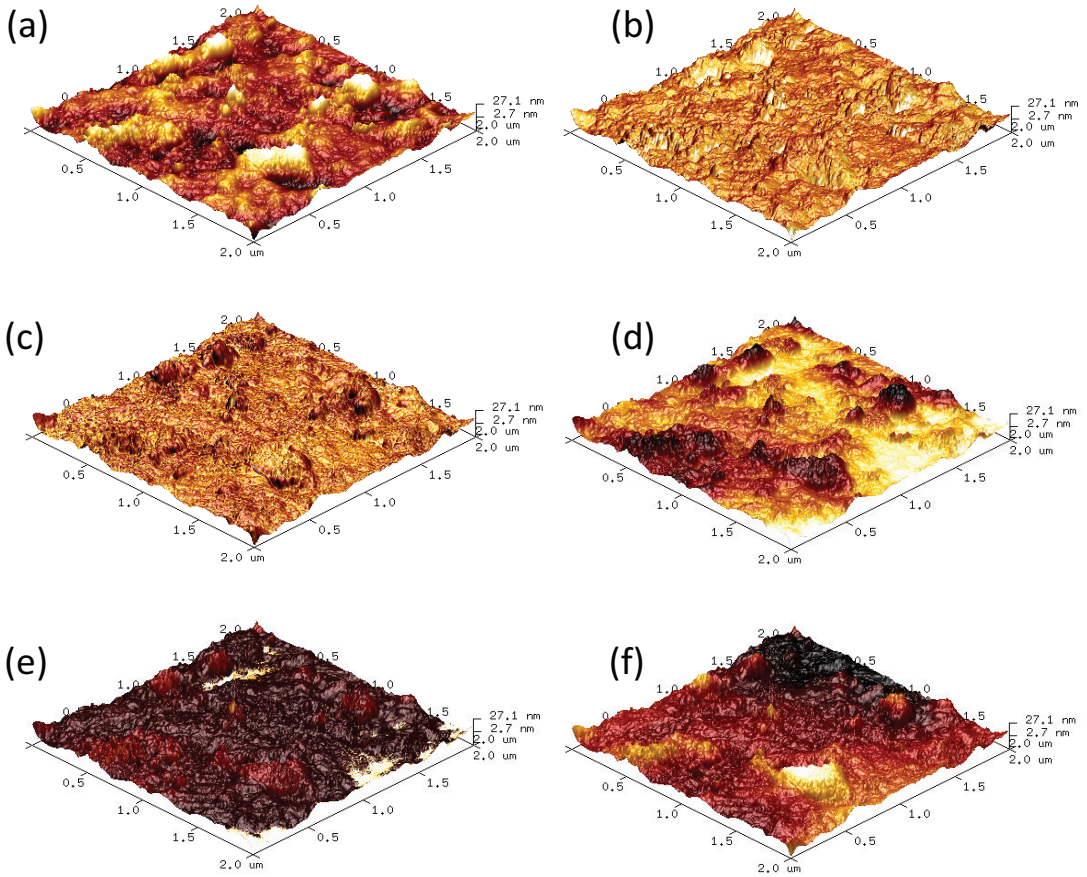

Fig. 4. (a) Height sensor, (b) peak force error, (c) LogDMT modulus, (d) adhesion, (e) deformation, and (f) dissipation images of fouled Aquaflex middle membrane. Scan area: 2 × 2 μm.

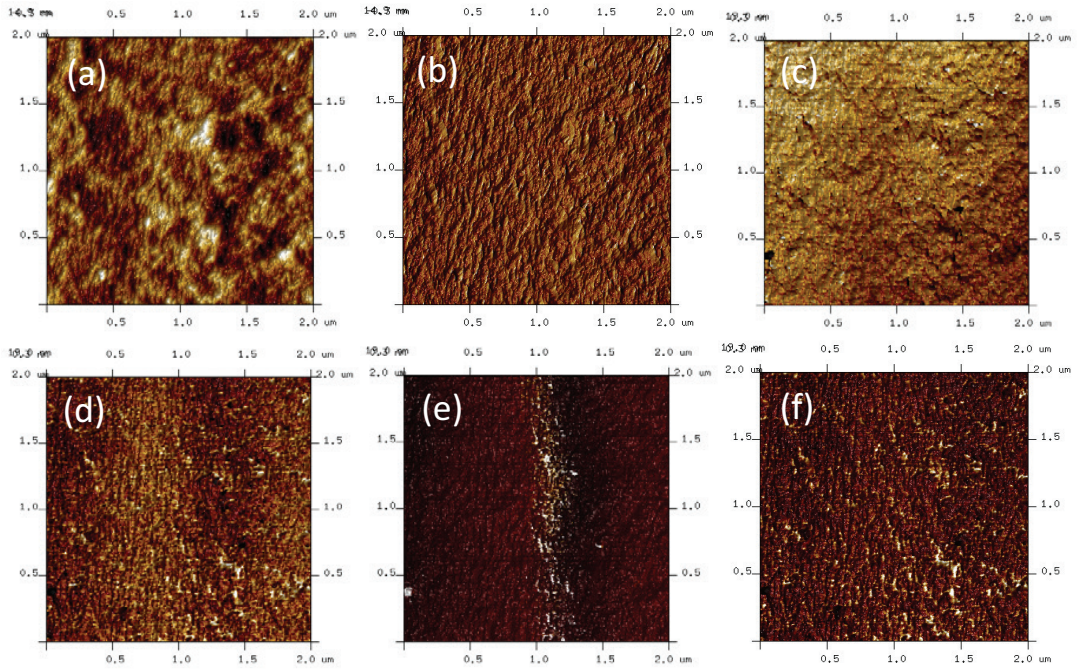

Fig. 5. (a) Height sensor, (b) peak force error, (c) LogDMT modulus, (d) adhesion, (e) deformation, and (f) dissipation images of Aquaflex bottom membrane. Scan area: 2 × 2 μm.

layers are considerably rougher, more adhesive, less elastic, and stiffer than the polymeric structures of virgin membranes. Previous studies have similarly reported the heterogeneous nature of foulants in water treatment systems [33]. The presence of these recalcitrant and heterogeneous foulants would be explained by the feed water quality of the secondary UF stage. The secondary UF stage was fed by a turbid water (i.e., 20–25 NTU, and containing coagulant flocs) with a significantly high total organic carbon (i.e., 22–28 mg C/L) and dissolved organic carbon (4–4.9 mg C/L) concentration (Table S3). Nevertheless, it was not possible to statistically discriminate between the foulant layers of harvested Aquaflex membranes (middle, top, or bottom modules) due to their high heterogeneity in nanomechanical properties. EDS spectra analysis of fouling material and Aquaflex virgin membrane surface was conducted (Table S4). Virgin membranes solely showed peaks of C, O, and S; which could be considered as representative of virgin membranes. Aquaflex top and Aquaflex middle showed additional peaks of Na, Cl, and K. Also, all the peaks in Aquaflex top and Aquaflex middle evidenced similar intensity. Nevertheless, only C, O, and S peaks were recorded in Aquaflex bottom, suggesting different fouling patterns. Due to the top-bottom filtration configuration, a lower fouling would be expected in Aquaflex bottom samples.

3.2.3. Mechanical properties of harvested hollow fiber membranes

The impact of operating conditions and feed quality on the nanomechanical properties of harvested membranes showing no adsorbed foulant layers was also studied (Fig. 5). The occurrence of clean membrane surfaces suggested the efficiency of the CEB cleaning process. First, the morphology of harvested membranes was investigated by AFM SoftTapping Mode™ technique. Harvested membranes evidenced a similar morphology at the nanoscale to that of virgin membranes (Figs. S7(a) and (b)). Specifically, polymeric structures and pores were clearly observed in all harvested membrane samples (Aquaflex top, Aquaflex middle, and Aquaflex bottom). As a supporting microscopy technique, SEM images were collected in the approximate locations where AFM images were recorded. AFM images were highly consistent with SEM micrographs, for example, some Aquaflex samples displayed parallel structural features possibly caused by use, cleaning, or manufacturing processes (Fig. S7(c)).

The nanomechanical properties of harvested membranes were statistically processed and analyzed by probability density functions (Table 1; Figs. S8 and S9). The roughness of harvested membranes was lower than those of Aquaflex virgin (Table 1), suggesting a probable polymer degradation. Additionally, the deformation of virgin membranes was slightly higher than Aquaflex top, Aquaflex middle, and Aquaflex bottom (i.e., 7.7, 4.0, 4.5, and 5.1 nm, respectively). On the other hand, the values of peak force and modulus of virgin and harvested membranes were similar in magnitude. However, the adhesion of the AFM probe to Aquaflex bottom and Aquaflex middle were slightly higher than to Aquaflex top and Aquaflex virgin (i.e., 0.52, 0.46, 0.37, and 0.36 nN, respectively); while the dissipation of virgin membranes was to some extent higher than those of harvested membranes. These results suggest UF membrane surfaces of lower deformation and higher adhesion after extended operation. Nevertheless, despite the differences in the magnitudes of deformation, adhesion, and dissipation among virgin and harvested membranes, the statistical analysis (i.e., probability distributions and variance) suggests that fouling and cleaning process did not significantly affect the surface properties of Aquaflex membranes. The operation conditions would have played an important role in this phenomenon. Despite the low feed quality of this secondary UF stage (Table S3), the three modules were only subjected to 37 CEBs and filtered a total volume of 2.155 m^3 during 449 d of operation. These conditions would not have been harsh enough to significantly impact the mechanical properties of the PES/PVP polymeric matrix of Aquaflex membranes. Remarkably, a previous similar QNM study observed a significant change in nanomechanical properties of UF hollow fiber membranes (three commercial Pentair X-Flow Xiga™ modules in horizontal dead-end configuration) subjected to 267 CEBs and filtering a total volume of 57.150 m^3 during 381 d of operation [30]. These results would suggest the key role of operation conditions on the surface characteristics of membranes.

3.3. Permeability of harvested hollow fiber membranes

The permeability of harvested membranes was measured and compared with those virgin membrane (Table S5). Virgin membranes showed a permeability of 968 lmbh. On the other hand, the permeability of Aquaflex top and Aquaflex middle were similar, as 775 and 782 lmbh, respectively. These values correspond to a performance of 80% and 81%, respectively. Conversely, the permeability of Aquaflex bottom was 956 lmbh, corresponding to a performance of 99% with respect to virgin membranes. The lower performance in the permeability tests observed for Aquaflex top and Aquaflex middle would be consistent to configuration of this secondary UF unit (i.e., operating in vertical dead-end top-bottom filtration); where the top and middle membrane modules would be subjected to a lower quality feed and would be consequently more impacted by fouling than the bottom membrane module. Following laboratory protocols and industrial practices, the efficiency of a cleaning process is measured by the extent of restoration of permeate flux [34]. Under this scenario, the 37 CEBs performed were not able to fully restore the permeability of these membrane modules, indicating the recalcitrant nature of the foulants as analyzed by QNM technique.

4. Conclusions: implications for water treatment processes

Few studies have investigated the long-term changes of polymeric UF membranes caused by fouling/cleaning agents (membrane ageing) in industrial processes with the use of macroscopic, spectroscopic, and nanomechanical methods [17]. In this regard, the current study conducted a QNM of the mechanical properties of hollow fiber membranes harvested after 449 d of operation and subjected to a low-quality feed. SEM and EDS, as well as permeability tests (i.e., measuring a macroscopic property of membranes) were used to study membrane surface changes and foulant layers. Results indicated that the recalcitrant and heterogeneous nature of the foulants absorbed on harvested membranes showed stiff polymeric structures (high modulus), low elastic properties,

and high adhesion and roughness. The strong affinity (irreversible adsorption) of these foulants towards the membrane surface would originate in the heterogeneity of their molecular constituents [35]; thus, altering membrane surface characteristics and influencing subsequent fouling behaviour as previously hypothesized [32]. Interestingly, the cleaning process and extended operation did not significantly affect the nanomechanical properties of membranes surfaces, as previously reported in similar investigations [30]. Despite the low-quality feed (i.e., turbid water with coagulant flocs and a high POC concentration), the three modules were only subjected to 37 CEBs and filtered a total volume of 2.155 m^3. These results indicate the importance of the operation conditions and feed quality on the long-term changes of polymeric UF membranes. Specifically, the frequency of backwash or cleaning/disinfection step would impact the physicochemical properties of the membrane (i.e., elasticity/plasticity of the membrane, surface zeta potential, membrane selectivity, and a loss of integrity) [17]. The knowledge compiled in the current study would assist in identifying research directions that are necessary to understand and strategically minimize membrane fouling/ageing. Future work should also consider the ageing of other elements of the module, and not restricted to membrane polymer analysis.

Acknowledgements

The financial support of the GenoMembran-project funded by The Swedish Water and Wastewater Association (Swedish Water Development, SVU), Norrvatten, and VIVAB is gratefully acknowledged. Pentair X-Flow is acknowledged for the provision of various test modules and general membrane investigations.

References

[1] J.N. Boyer, J.W. Fourqurean, R.D. Jones, Seasonal and long-term trends in the water quality of Florida Bay (1989–1997), Estuaries, 22 (1999) 417–430.
[2] H. Huang, K. Schwab, J.G. Jacangelo, Pretreatment for low pressure membranes in water treatment: a review, Environ. Sci. Technol., 43 (2009) 3011–3019.
[3] N.D. Lawrence, M. Iyer, M.W. Hickey, G.W. Stevens, J.M. Perera, Mastering membrane cleaning, Austr. J. Dairy Technol., 53 (1998) 193–194.
[4] X. Cui, K.-H. Choo, Natural organic matter removal and fouling control in low-pressure membrane filtration for water treatment, Environ. Eng. Res., 19 (2014) 1–8.
[5] C. Hwang, S.W. Kranser, G. Amy, A. Bruchet, J.P. Croue, A. Leenheer Jerry, Polar NOM: Characterization, DBPs, Treatment, AWWA Research Foundation, 2001.
[6] M. Nyström, K. Ruohomäki, L. Kaipia, Humic acid as a fouling agent in filtration, Desalination, 106 (1996) 79–87.
[7] N. Lee, G. Amy, J.-P. Croué, H. Buisson, Identification and understanding of fouling in low-pressure membrane (MF/UF) filtration by natural organic matter (NOM), Water Res., 38 (2004) 4511–4523.
[8] K. Rajesha, I.A.F. Fouling control on microfiltration/ultrafiltration membranes: effects of morphology, hydrophilicity, and charge, J. Appl. Polym. Sci., 132 (2015) 1–20.
[9] K. Kimura, Y. Hane, Y. Watanabe, G. Amy, N. Ohkuma, Irreversible membrane fouling during ultrafiltration of surface water, Water Res., 38 (2004) 3431–3441.
[10] H. Yamamura, K. Okimoto, K. Kimura, Y. Watanabe, Influence of calcium on the evolution of irreversible fouling in microfiltration/ultrafiltration membranes, J. Water Supply: Res. Technol. - Aqua, 56 (2007) 425.
[11] X. Shi, R. Field, N. Hankins, Review of fouling by mixed feeds in membrane filtration applied to water purification, Desal. Wat. Treat., 35 (2011) 68–81.
[12] D. Jermann, W. Pronk, S. Meylan, M. Boller, Interplay of different NOM fouling mechanisms during ultrafiltration for drinking water production, Water Res., 41 (2007) 1713–1722.
[13] G.F. Crozes, J.G. Jacangelo, C. Anselme, J.M. Laîné, Impact of ultrafiltration operating conditions on membrane irreversible fouling, J. Membr. Sci., 124 (1997) 63–76.
[14] X. Shi, G. Tal, N.P. Hankins, V. Gitis, Fouling and cleaning of ultrafiltration membranes: a review, J. Water Process Eng., 1 (2014) 121–138.
[15] A. Maartens, E.P. Jacobs, P. Swart, UF of pulp and paper effluent: membrane fouling-prevention and cleaning, J. Membr. Sci., 209 (2002) 81–92.
[16] H. Huang, N. Lee, T. Young, A. Gary, J.C. Lozier, J.G. Jacangelo, Natural organic matter fouling of low-pressure, hollow-fiber membranes: effects of NOM source and hydrodynamic conditions, Water Res., 41 (2007) 3823–3832.
[17] C. Regula, E. Carretier, Y. Wyart, G. Gésan-Guiziou, A. Vincent, D. Boudot, P. Moulin, Chemical cleaning/disinfection and ageing of organic UF membranes: a review, Water Res., 56 (2014) 325–365.
[18] S.H. Wolff, A.L. Zydney, Effect of bleach on the transport characteristics of polysulfone hemodialyzers, J. Membr. Sci., 243 (2004) 389–399.
[19] A. Ettori, E. Gaudichet-Maurin, J.-C. Schrotter, P. Aimar, C. Causserand, Permeability and chemical analysis of aromatic polyamide based membranes exposed to sodium hypochlorite, J. Membr. Sci., 375 (2011) 220–230.
[20] K. Yadav, K. Morison, M.P. Staiger, Effects of hypochlorite treatment on the surface morphology and mechanical properties of polyethersulfone ultrafiltration membranes, Polym. Degrad. Stab., 94 (2009) 1955–1961.
[21] M. Rabiller-Baudry, G. Gésan-Guiziou, C. Causserand, éditrices, Le nettoyage des équipements à membrane: une étape clef dans la production durable, Applications: Fluides alimentaires, eau potables, eaux usées dans Cahiers du Club Français des Membranes, 2012.
[22] L. Bégoin, M. Rabiller-Baudry, B. Chaufer, C. Faille, P. Blanpain-Avet, T. Bénézech, T. Doneva, Methodology of analysis of a spiral-wound module. Application to PES membrane for ultrafiltration of skimmed milk, Desalination, 192 (2006) 40–53.
[23] L. Bégoin, M. Rabiller-Baudry, B. Chaufer, M.-C. Hautbois, T. Doneva, Ageing of PES industrial spiral-wound membranes in acid whey ultrafiltration, Desalination, 192 (2006) 25–39.
[24] N. Porcelli, S. Judd, Chemical cleaning of potable water membranes: a review, Sep. Purif. Technol., 71 (2010) 137–143.
[25] C. Regula, E. Carretier, Y. Wyart, M. Sergent, G. Gésan-Guiziou, D. Ferry, A. Vincent, D. Boudot, P. Moulin, Drinking water ultrafiltration: state of the art and experimental designs approach, Desal. Wat. Treat., 51 (2013) 4892–4900.
[26] S. Rouaix, C. Causserand, P. Aimar, Experimental study of the effects of hypochlorite on polysulfone membrane properties, J. Membr. Sci., 277 (2006) 137–147.
[27] S. Robinson, S.Z. Abdullah, P. Bérubé, P. Le-Clech, Ageing of membranes for water treatment: linking changes to performance, J. Membr. Sci., 503 (2016) 177–187.
[28] H.J. Butt, B. Cappella, M. Kappl, Force measurements with the atomic force microscope: technique, interpretation and applications, Surf. Sci. Rep., 59 (2005) 1–152.
[29] B.V. Derjaguin, V.M. Muller, Y.U.P. Toporov, Effect of contact deformations on the adhesion of particles, J. Colloid Interface Sci., 53 (1975) 314–326.
[30] L. Gutierrez, A. Keucken, C. Aubry, N. Zaouri, B. Teychene, J.-P. Croue, Impact of operation conditions, foulant adsorption, and chemical cleaning on the nanomechanical properties of ultrafiltration hollow fiber membranes, Colloids Surf., A, 549 (2018) 34–42.
[31] J.A. Brant, K.M. Johnson, A.E. Childress, Characterizing NF and RO membrane surface heterogeneity using chemical force microscopy, Colloids Surf., A, 280 (2006) 45–57.
[32] L. Gutierrez, C. Aubry, R. Valladares Linares, J.-P. Croue, Natural organic matter interactions with polyamide and

polysulfone membranes: formation of conditioning film, Colloids Surf., A, 477 (2015) 1–8.
[33] M.T. Khan, C.-L. de O Manes, C. Aubry, L. Gutierrez, J.P. Croue, Kinetic study of seawater reverse osmosis membrane fouling, Environ. Sci. Technol., 47 (2013) 10884–10894.
[34] A. Maartens, P. Swart, E.P. Jacobs, Removal of natural organic matter by ultrafiltration: characterisation, fouling and cleaning, Water Sci. Technol., 40 (1999) 113–120.
[35] K.L. Jones, C.R. O'Melia, Protein and humic acid adsorption onto hydrophilic membrane surfaces: effects of pH and ionic strength, J. Membr. Sci., 165 (2000) 31–46.

Supporting information

Table S1
Operating conditions and process parameters during long-term pilot trials

Parameters	Unit	UF secondary
Maximum filtration time (t_F)	min	60
Maximum filtration volume	m^3	1.65
Filtration flux (J_F)	L m^{-2} h^{-1}	45
Cross flow velocity (v_{CF})	m s^{-1}	0.5
Recovery during filtration (R)	%	100
Backwash time (t_{BW})	s	30
Backwash flux (J_{BW})	L m^{-2} h^{-1}	250
CEB interval (t_{CEFF})	d	5
CEB1 dosing solution (caustic)	–	250–300 ppm NaOCl at pH 12.2 with NaOH
CEB2 dosing solution (acidic)	–	475 mg/L H_2SO_4 at pH 2.4
Soak time CEB (t_{SOAK})	min	10

Table S2
Membrane key performance parameters during pilot trials

Parameters	Unit	UF secondary
Permeability	L/m^2 h bar at 20°C	600–220
Transmembrane pressure	bar	0.12–0.25
Total number of CEBs	–	37
Module age before replacement	months	14
Installation date	–	08.05.2015
Autopsy date	–	01.08.2016
Total filtration volume (feed water)	m^3	2.155[a]

[a]4.8 m^3/d × 449 d.

Table S3
Average feed water quality of secondary UF stage

Parameters	Unit	Range (UF stage 2)
Temperature	°C	3.8–4.9
pH	–	7.0–7.3
Turbidity	NTU	20.0–25.0
Hardness	°dH	1.4–1.7
Alkalinity	mg/L HCO_3)	15–18
COD	mg/L O_2)	19–34
TOC	mg C/L)	22.0–28.0
DOC	mg C/L	4.0–4.9
UV_{254}	–	1.530–6.370
Pt-Co	mg Pt/L	15–25
Conductivity	µS/cm	100–107
Iron	mg/L Fe	0.480–0.680
Manganese	mg/L Mn)	0.037–0.048
Calcium	mg/L Ca^{2+}	6.6–8.3
Magnesium	mg/L Mg^{2+}	2.2–2.5
Sodium	mg/L Na^+	8.1–9.8
Ammonium	mg/L $NH4^+$	0.01–0.10
Sulphate	mg/L SO_4^{2-}	8.5–10.0
Nitrate	mg/L NO_3^-	1.4–1.6

Table S5
Permeability of virgin and harvested membranes

Parameter	Units	Aquaflex membranes			
		Virgin	Top	Middle	Bottom
Permeability	lmbh	968	775	782	956
Performance	%		80	81	99

Table S4
EDS analysis of virgin and harvested membranes

Sample	%C	%O	%Na	%Al	%Si	%S	%Cl	%K
Aquaflex virgin	67	14				19		
Aquaflex top	58	7	4			23	7	2
Aquaflex middle	55	7	3			21	10	4
Aquaflex bottom	65	9				26		

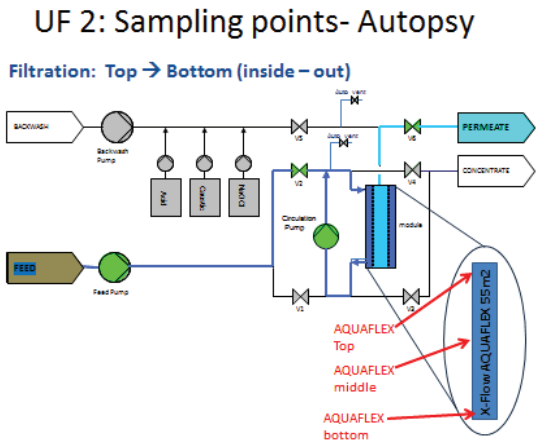

Fig. S1. Sampling points for membrane autopsy for Aquaflex membranes.

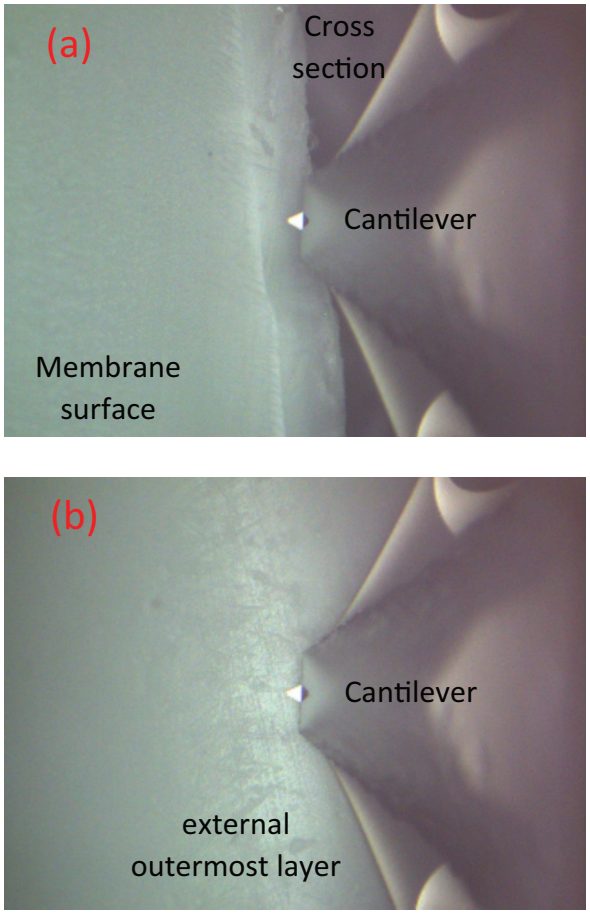

Fig. S2. Area in hollow fiber membrane selected for AFM analysis: (a) membrane surface and cross section, and (b) the external outermost layer of the hollow fiber membrane (i.e., housing material). Images were acquired using the high-resolution camera of the AFM.

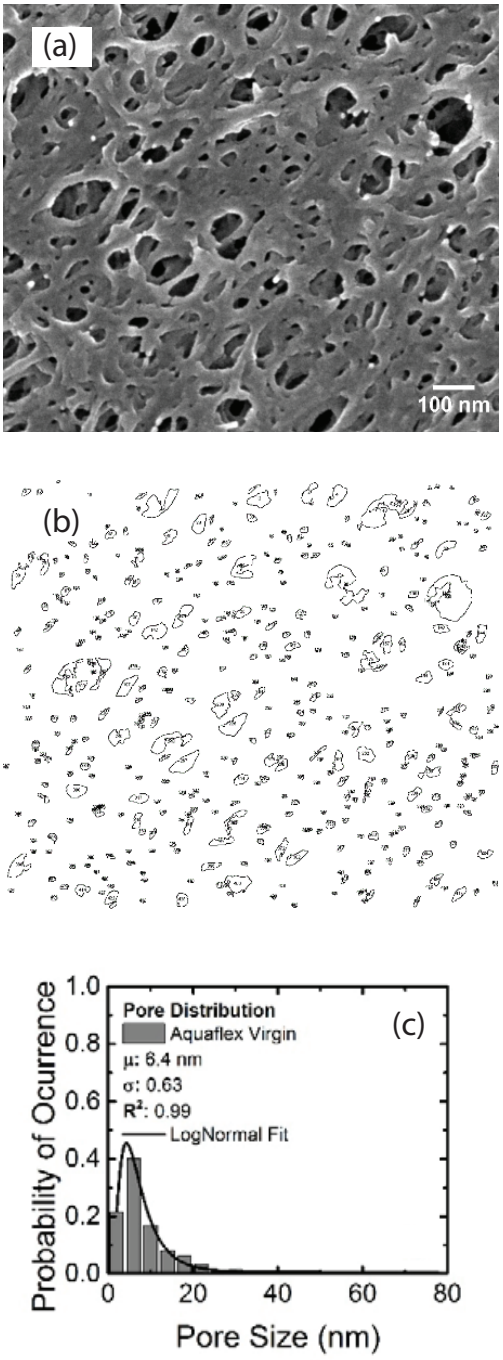

Fig. S3. (a) SEM image of Aquaflex virgin membrane surface. (b) Pores discriminated from membrane surface by ImageJ software. (c) Probability density functions describing the pore size distribution of Aquaflex virgin.

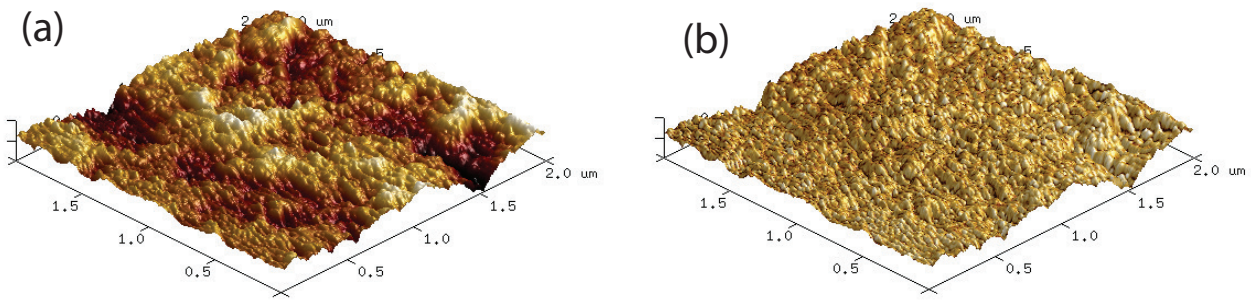

Fig. S4. 3D-height sensor of (a) topography and (b) phase images of Aquaflex Virgin. Images were acquired in tapping mode in air. Scan area: 2 × 2 μm.

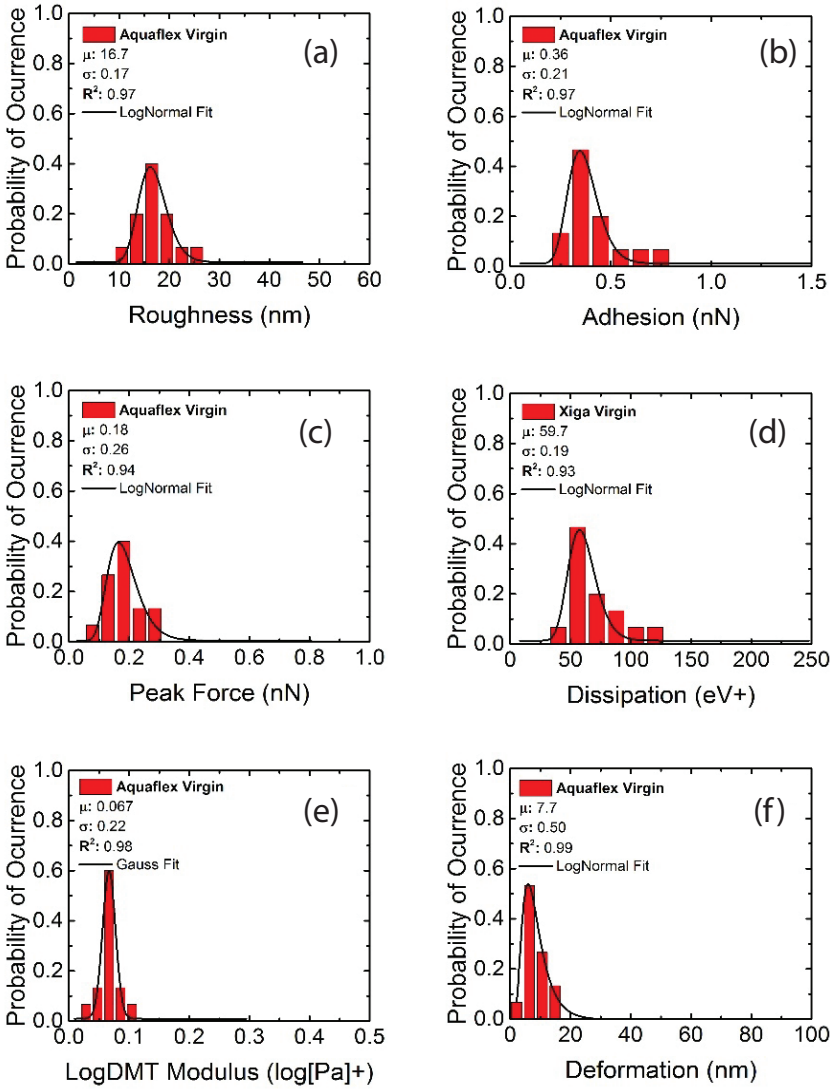

Fig. S5. Probability density functions describing (a) roughness, (b) adhesion, (c) peak force error, (d) dissipation, (e) LogDMT modulus, and (f) deformation of Aquaflex virgin membrane.

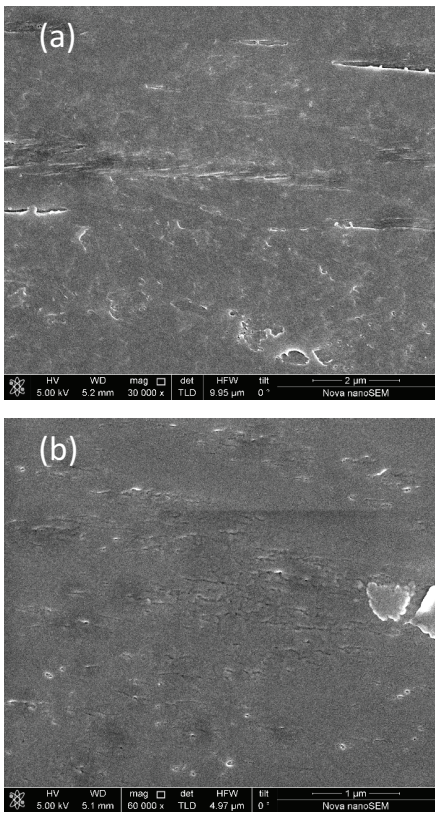

Fig. S6. SEM images of fouled (a) Aquaflex bottom and (b) Aquaflex middle membranes showing micro-cracks.

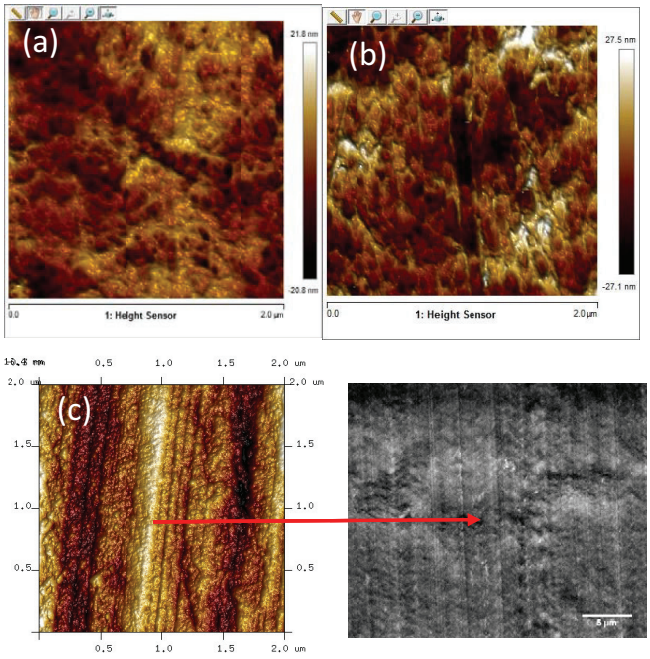

Fig. S7. High resolution images acquired in soft-tapping mode of (a) Aquaflex virgin and (b) Aquaflex middle. QNM-height sensor and SEM images depicting the morphology of (c) Aquaflex bottom.

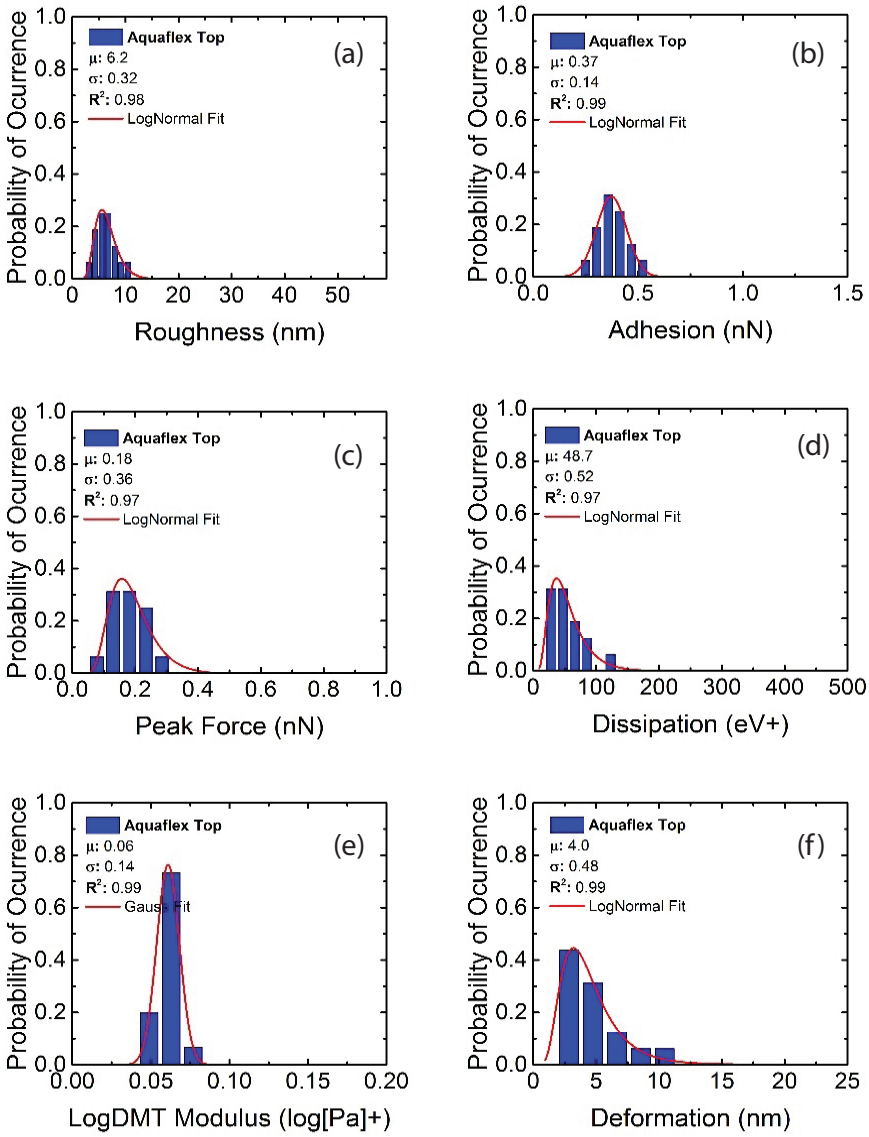

Fig. S8. Probability density functions describing (a) roughness, (b) adhesion, (c) peak force error, (d) dissipation, (e) LogDMT modulus, and (f) deformation of Aquaflex top membrane.

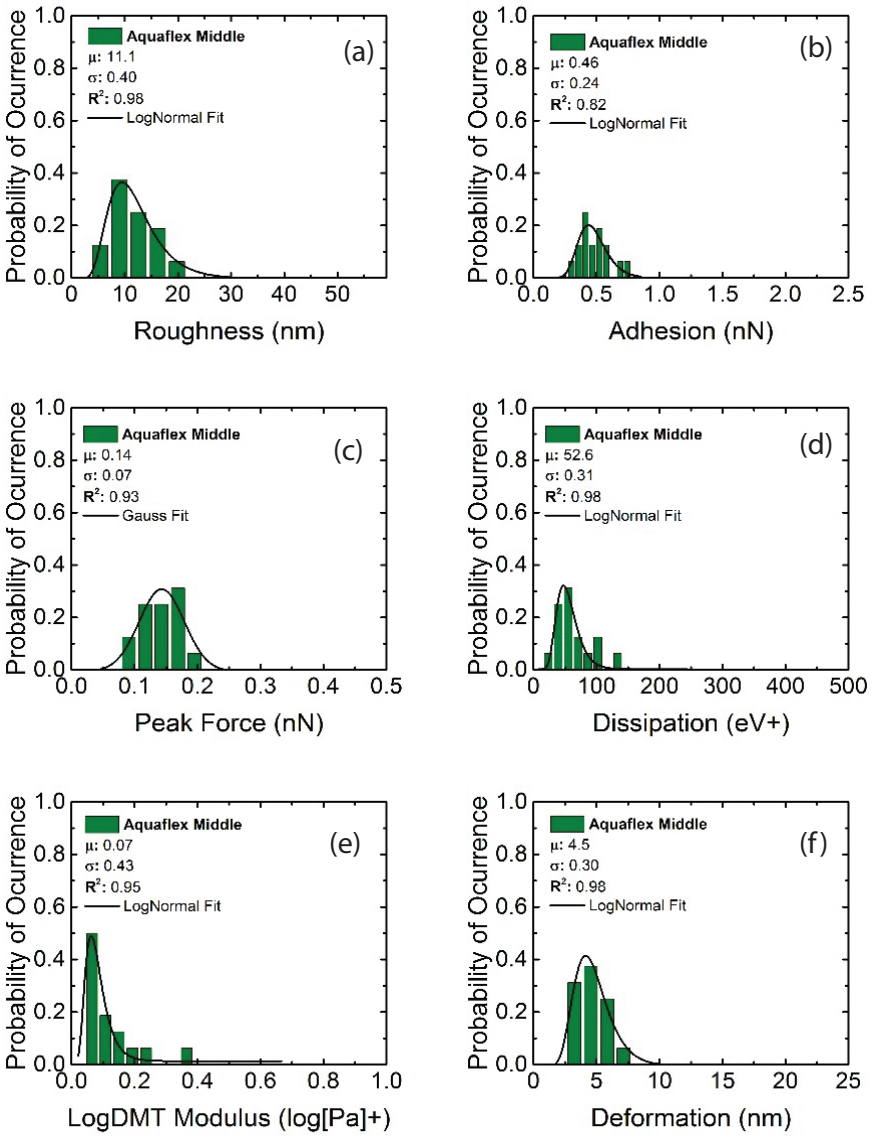

Fig. S9. Probability density functions describing (a) roughness, (b) adhesion, (c) peak force error, (d) dissipation, (e) LogDMT modulus, and (f) deformation of Aquaflex middle membrane.